



AgBr-loaded hollow porous carbon nitride with ultrahigh activity as visible light photocatalysts for water remediation

Xuewen Li, Dongyun Chen*, Najun Li, Qingfeng Xu, Hua Li, Jinghui He, Jianmei Lu*

College of Chemistry, Chemical Engineering and Materials Science, Collaborative Innovation Center of Suzhou Nano Science and Technology, Soochow University, Suzhou, 215123, China



ARTICLE INFO

Keywords:

Carbon nitride
Hollow porous nanospheres
AgBr-loaded
OG degradation

ABSTRACT

Nowadays, the lack of water resources is mainly due to frequent industrial discharge of dyes wastewater such as azo dyes, so the demand of photocatalysts with rapid degradation rate is growing. We report the synthesis of a new morphology of AgBr-loaded carbon nitride nanoparticles with hollow porous nanostructures, HCNS/AgBr, which was prepared by a hard-templating and the deposition-precipitation method. The morphology, surface elements and optical properties of the HCNS/AgBr hybrids were characterized using transmission electron microscopy (TEM), X-ray photoemission spectroscopy (XPS) and photoluminescence (PL) spectroscopy. Different mass ratios of HCNS/AgBr were prepared and HCNS/AgBr60 showed the highest photoactivity for Orange G (OG) dye degradation under visible light irradiation. Degradation efficiency was shown to reach 97% within 10 min, which could be attributed to the formation of a heterojunction structure and the high separation efficiency of holes and electrons, meanwhile the mechanism was evidenced by free radical and hole scavenging experiments. The results demonstrate the potential application of this new photocatalyst in the removal of dye from wastewater.

1. Introduction

Rapid industrialization has made life more convenient for many but has also given rise to environmental pollution, for example of the air, soil and water. Environmental pollution is a global issue that draws the attention of countries worldwide due in part to its negative impact on the health of the human population [1–3]. The discharge of untreated dye wastewater is one of the headstreams of water pollution. The textile and printing industries use large quantities of synthetic dyes [4], with azo dyes being particularly difficult to remove due to their stable, highly-substituted aromatic structures [5,6]. Consequently, several techniques for dye treatment have been developed, such as oxidation [7], adsorption [8], biological treatments [9], electrochemical methods [10] and photocatalysis [11]. Visible light-induced semiconductor photocatalysts, which are environmentally friendly and recyclable, have been the subject of research for many years; however, despite their numerous advantages, their degradation rates are not ideal, which has led to a need for catalyst optimization.

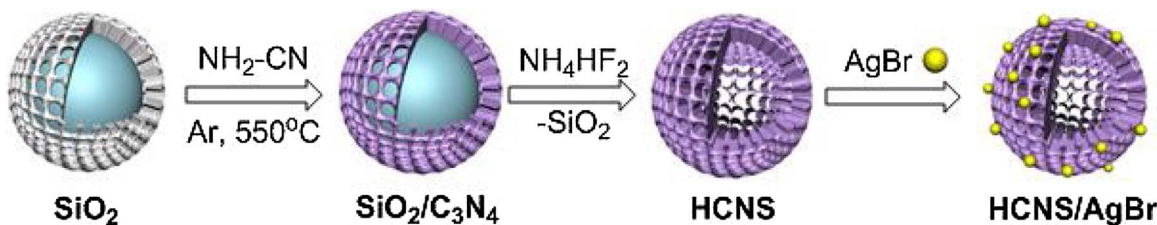
Visible-response semiconductors have attracted interest since TiO_2 was first reported to show photocatalytic activity. Recently, Lin Dong and his co-workers have synthesized metal oxide clusters modified TiO_2 Nanosheets (TM- TiO_2 Nanosheets) for the photocatalytic O_2 evolution

from water [12] and TiO_2 nanocrystals with different crystal forms and crystal facets for the photocatalytic selective reduction and selective oxidation [13]. The ability of photocatalysts such as ZnO [14,15], BiPO_4 [16], Nb_2O_5 [17], Bi_2O_3 [18], $(\text{BiO})_2\text{CO}_3$ [19], Fe_2O_3 [20,21] and carbon nitride (C_3N_4) [22] to degrade synthetic dyes has been studied, however degradation rates are slow, approximately 2 h duration, owing to inefficient utilization of solar energy and fast recombination rates of electron-hole pairs. The introduction of additional elements, known as doping, is considered a means of adjusting the electronic, optical, luminescent and other physical properties of a material. To improve the photocatalytic rate by increasing the separation efficiency of electron-hole pairs, many hybrid materials such as N-doped TiO_2 [23], Fe^{3+} doped TiO_2 [24], graphene–gold nanocomposites [25], Mn-doped ZnO [26], BiOI/TiO_2 [27], Cu_2O -reduced graphene oxide (rGO) composites with different crystal facets [28], c- CeO_2 /g- C_3N_4 [29] and $\text{AgX}/\text{graphite-like C}_3\text{N}_4$ [30] have been investigated.

Graphitic carbon nitride (g- C_3N_4), a metal-free, conjugated, polymeric semiconductor, has caused a research boom due to its high physicochemical stability, favorable electronic band structure and facile synthesis [31–33] by thermal polymerization of abundant nitrogen-rich precursors such as melamine [34,35], urea [36,37], thiourea [38,39], cyanamide, dicyandiamide [40–42] and ammonium

* Corresponding authors.

E-mail addresses: dychen@suda.edu.cn (D. Chen), lujm@suda.edu.cn (J. Lu).



Scheme 1. Schematic illustration of HCNS and HCNS/AgBr composite synthesis.

thiocyanate [43]. It has been shown that the basic units that yield allotropes of $\text{g-C}_3\text{N}_4$ are triazine (C_3N_3) and tri-*s*-triazine/heptazine (C_6N_7) rings. Of all phases of C_3N_4 , which include α - C_3N_4 , β - C_3N_4 , cubic C_3N_4 , pseudocubic C_3N_4 , $\text{g-}o$ -triazine, $\text{g-}h$ -triazine and $\text{g-}h$ -heptazine [44]; tri-*s*-triazine-based $\text{g-C}_3\text{N}_4$ is the most stable under ambient conditions [45]. However, owing to a high recombination rate of charge carriers, low electrical conductivity, and low specific surface area ($7.7 \text{ m}^2 \text{ g}^{-1}$) in bulk C_3N_4 , native C_3N_4 still has limitations in practical applications. Engineering C_3N_4 nanostructure to enlarge the specific surface area is therefore one way to optimize photoactivity.

In this study, hollow, porous carbon nitride nanospheres (HCNS) coupled with AgBr nanoparticles (HCNS/AgBr), were fabricated for the degradation of organic dyes. The preparation of HCNS/AgBr is outlined in Scheme 1. First, silica particles with a solid core surrounded by a thin mesoporous shell were synthesized using the Stöber method. Cyanamide was then loaded into the pores of the silica shells and C_3N_4 /silica nanocomposites were obtained after calcination at 550°C under a stream of Ar. The sacrificial silica templates were then removed using NH_4HF_2 solution. Finally, AgBr nanoparticles were loaded onto the surface of the HCNS using the deposition-precipitation method. The obtained HCNS/AgBr material shows a high photocatalytic performance, with the efficiency for OG degradation reaching 97% within 10 min. This is attributed to the structure of the hollow, porous carbon nitride nanospheres, which leads to an increase in specific surface area compared with bulk C_3N_4 . The BET surface area was $16.9293 \text{ m}^2 \text{ g}^{-1}$ for HCNS, approximately twice that of bulk C_3N_4 . There is also thought to be a decrease in the recombination rate of charge carriers.

2. Experimental section

2.1. Materials

Tetraethyl orthosilicate (TEOS), trimethoxyoctadecylsilane (C_{18}TMOS), cyanamide were purchased from Sigma Aldrich. Ethanol, aqueous ammonia (28 wt%), ammonium acid fluoride, hydrochloric acid, silver nitrate, sodium bromide were purchased from Sinopharm Chemical Reagent Co. Ltd (China).

2.2. Instrumentation

Scanning electron microscopy (SEM) (Hitachi S-4700) and Transmission electron microscopy (TEM) (Tecnai G200) were used to examine the morphologies and structures of the samples. The optical properties were determined by UV-visible diffuse reflectance spectroscopy (UV-vis DRS, Shimadzu UV-3600). X-ray diffraction (XRD) (X' Pert-Pro MPD) was performed to analyze the crystal phase. X-ray photoelectron spectroscopy (XPS) of the sample was examined using an X-ray photoelectron spectrometer (ESCALAB MK II) with Al-K α radiation. The photoluminescence (PL) spectra of the samples were recorded by using a fluorescence spectrophotometer (FLS920) with an excitation wavelength of 360 nm. Electrochemical measurements were conducted with a CHI 660B electrochemical system (Shanghai, China) according to the literature.

2.3. Synthesis of the SiO_2 template

Core-shell structured silica templates were synthesized according to the Stöber method, a homodisperse silica core was covered with a loose mesoporous silica shell. Typically, 10 mL ultrapure water and 3.50 g aqueous ammonia (28 wt %) were added into round-bottom flask including 58.5 g ethanol solution. After stirring for 30 min at 30°C , 5.6 mL TEOS was added into the above-prepared mixture quickly with magnetic stirring and the mixture kept stirring for 1 h to yield uniform silica spheres. To create a mesoporous silica shell, a mixture solution containing 5.83 g TEOS and 2.62 g C_{18}TMOS was added into the above solution drop by drop with vigorous stirring. Then, the mixed solution was kept static for 3 h to promote the cohydrolysis and condensation at 30°C . The resulting reaction solution was centrifuged, dried at 70°C and calcined at 550°C for 6 h in the air. The obtained white powder was neutralized with a 1-M HCl solution, washed with ethanol and dried at 80°C overnight [46].

2.4. Synthesis of HCNS

The core-shell nanostructured silica particles were used as a template to synthesize the hollow carbon nitride spheres. In detail, 1 g SiO_2 powder was added into 5 g thawed cyanamide in a flask, which was vacuumized for 30 min and mixed for 2 h at 60°C . Then, the mixture was stirred all night before ultrasonic treatment for 4 h at 60°C . The resultant was centrifuged and dried in air to obtain a white solid that was grinded and put into a crucible to calcine at 550°C under flowing Ar for 4 h with a ramp rate of 5°C min^{-1} . The obtained light yellow mixed power was etched with 4 M NH_4HF_2 for 12 h to remove SiO_2 templates. The turbid liquid was centrifuged and washed with distilled water and ethanol for three times respectively. Finally, the yellow powers were collected by drying at 80°C in a vacuum oven overnight [46].

2.5. AgBr nanoparticles loaded in HCNS

To prepare HCNS/AgBr composite photocatalyst, the deposition-precipitation method was adopted. A given amount of HCNS as the substrate was dispersed in 8 mL deionized water, and the suspension was sonicated for 30 min. Then, 85 mg AgNO_3 was added into above suspension and stirred for 1 h in the dark. Then, 51.5 mg NaBr was dissolved in ultrapure water and added dropwise into the above mixture, which was stirred for 3 h in the dark. The resulting products were centrifuged and washed with ultrapure water and acetone for three times then dried at 60°C . Different mass ratios of the AgBr versus HCNS samples were prepared and discussed to study the effect of photocatalysts, which was denoted as HCNS/AgBr10 (AgBr: HCNS = 10 wt %), HCNS/AgBr30, HCNS/AgBr60, HCNS/AgBr90, respectively [47].

2.6. Photocatalytic activity

The adsorption and photocatalytic activity of as-prepared photocatalysts were evaluated by the degradation of OG under visible light irradiation by a 300 W Xe lamp with a 400 nm cutoff filter. In a typical experiment, 0.1 g photocatalysts were put into 100 mL OG (25 mg/L) in

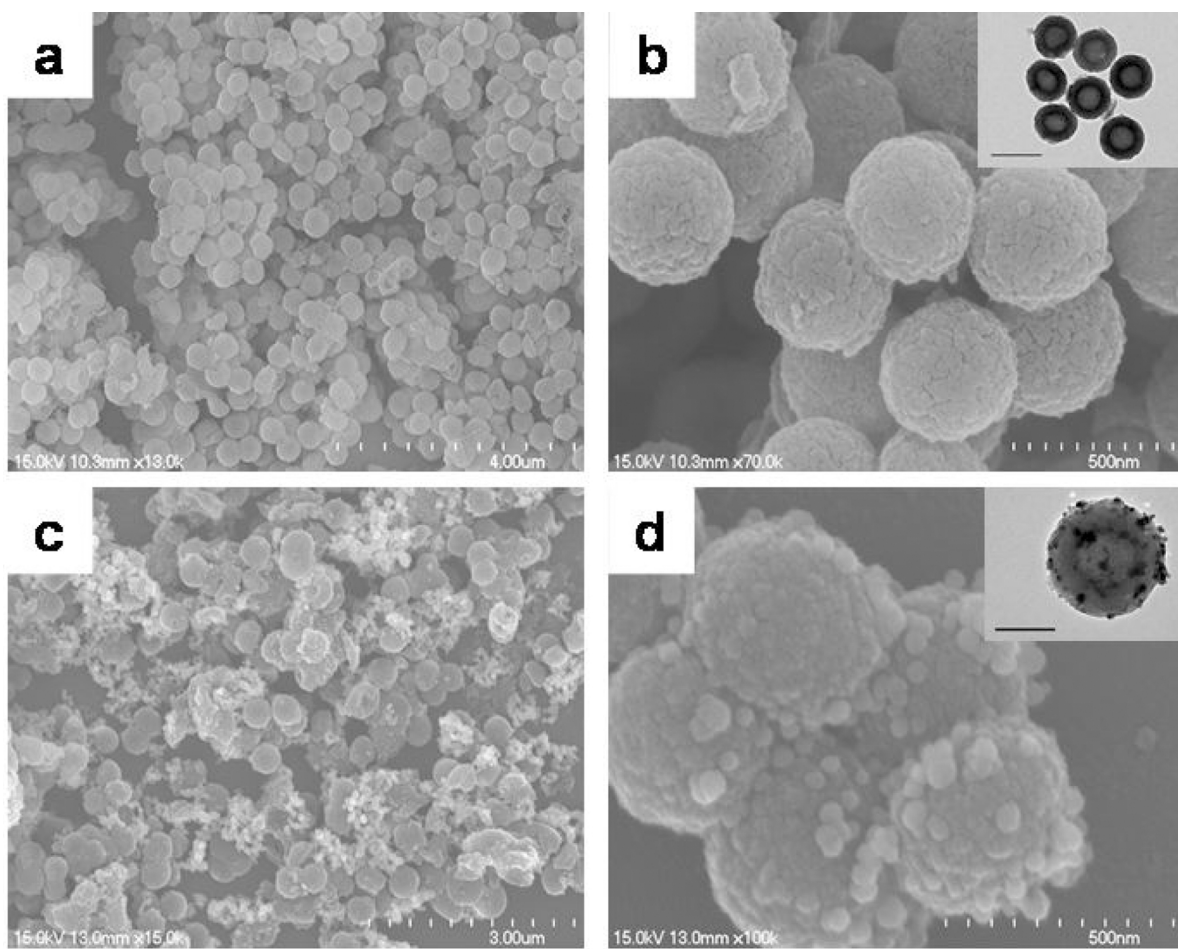


Fig. 1. SEM (a) and TEM (b) images of HCNS, the scale bar of TEM image represents 0.5 μ m and SEM (c) and TEM (d) images of HCNS/AgBr60, the scale bar of the TEM represents 0.2 μ m.

a reactor. To make sure that the OG dye could reach the equilibrium of absorption-desorption on the surface of the photocatalyst, prior to irradiation, the suspension were stirred for 30 min at 30 °C in the dark. Then, all the procedures were carried out at 30 °C under constant stirring. 3 mL suspension was sampled in certain intervals and centrifuged, the liquid was tested by an UV-vis spectroscopy according to its absorbance at 476 nm. For comparison, the same experiment was repeated with C₃N₄/AgBr60 (AgBr: bulk C₃N₄ = 60 wt %).

3. Results and discussion

3.1. Characterization

3.1.1. Morphology

Scanning electron microscopy (SEM) and transmission electron microscopy (TEM) were used to determine the morphology and structure of the samples. HCNS was prepared using sacrificial silica templates, known as the hard-templating approach. As shown in Fig. 1a and b, homodisperse carbon nitride nanospheres were successfully synthesized. The hollow nature of the structures is supported by the TEM image (Fig. 1b). It can be seen that a small number of the carbon nitride shells are not truly spherical. This is probably due to the collapse of the carbon nitride structures during silica template removal. AgBr nanoparticles were loaded onto the surface of the HCNS, four different mass ratios of HCNS/AgBr samples (Fig. S1) were prepared in order to further investigate the photocatalytic performance, resulting in a relatively uniform particle distribution as can be seen in Fig. 1c and d. The TEM image (Fig. 1d) reveals that the hollow structure was not compromised by the introduction of AgBr nanoparticles.

3.1.2. Structural information

XPS was used to analyze the surface chemistry of HCNS/AgBr60. The survey XPS spectrum shown in Fig. 2a, reveals the presence of C, N, Ag, Br and O elements. The O 1s peaks are attributed to atmospheric oxygen. The high resolution XPS spectra are shown in Fig. 2b–e. For Ag 3d, two individual peaks were obtained at 367.6 eV and 373.6 eV, which could be ascribed to the Ag⁺ in AgBr and the binding energies of Ag 3d_{5/2} and Ag 3d_{3/2}, respectively. For Br 3d, two peaks at 68.1 eV and 69.0 eV correspond to Br 3d_{5/2} and Br 3d_{3/2}, respectively. As can be seen in Fig. 2d, the C 1s spectrum shows two major peaks at 284.8 eV and 288.1 eV, which are attributed to the carbon atoms (sp² C–C bonds) and the sp²-hybridized carbon in the aromatic ring including N (N=C=N), respectively. The two peaks of the N 1s spectrum (Fig. 2e), can be deconvoluted into three peaks. The main peak at 398.6 eV is ascribed to the sp²-bonded N in triazine rings (C=N=C) with the other peaks at 399.5 eV and 400.7 eV, corresponding to the tertiary nitrogen N–(C)₃ groups and amino groups carrying hydrogen (C–N–H), respectively [47].

XRD was used to investigate the chemical structure of as-prepared samples. As shown in Fig. 3a, the characteristic peak of HCNS can be seen at 27.7° and is indexed as (002). This corresponds to interlayer stacking of the aromatic structure with a stacking distance of 0.323 nm. AgBr exhibits identifiable peaks at 26.7°, 31.2°, 44.5°, 55.1°, 64.7° and 73.4° which are indexed as (111), (200), (220), (222), (400) and (420), respectively [48]. As AgBr content increases, the intensity of the HCNS peak becomes weaker, which are hardly found in the diffraction peaks of HCNS/AgBr90, meanwhile, the characteristic peaks of the AgBr become manifest and stronger. In general, addition of AgBr did not change the crystal structure of the HCNS.

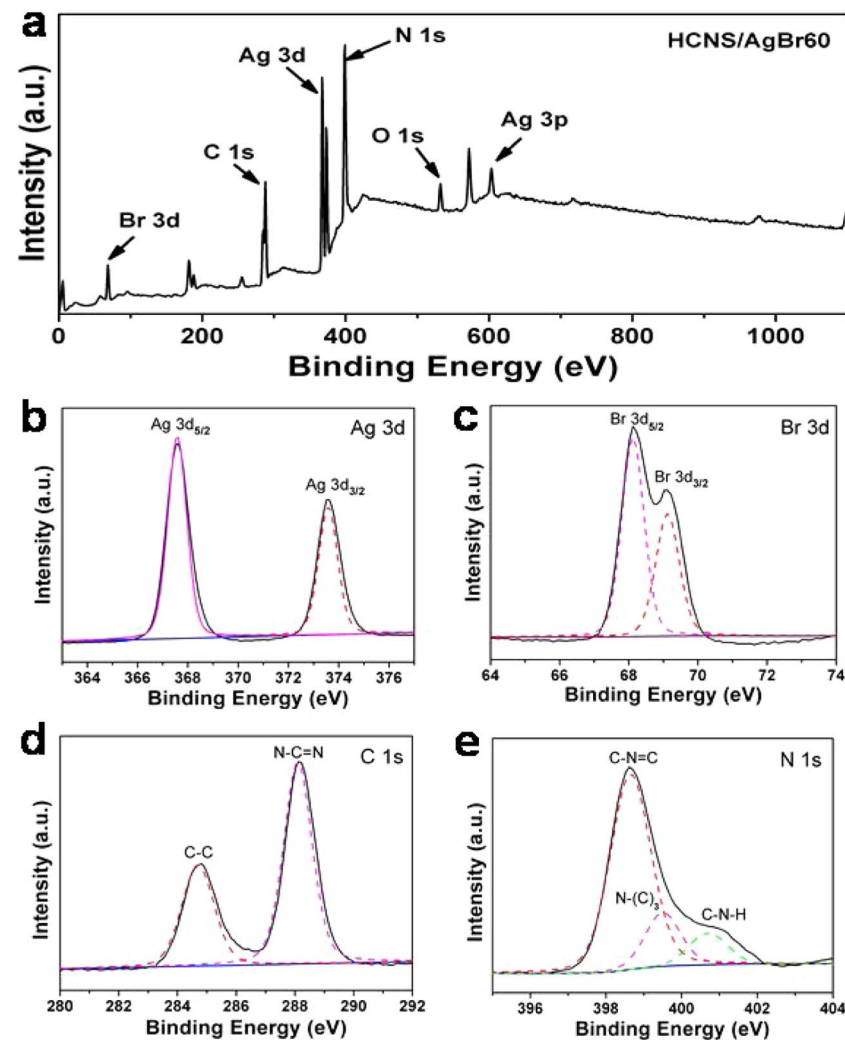


Fig. 2. (a) Survey XPS spectrum, (b) Ag 3d, (c) Br 3d, (d) C 1s and (e) N 1s XPS spectra of HCNS/AgBr60 nanocomposite.

3.1.3. Optical properties

Optical properties are an important factor in photocatalyst performance. The UV-vis diffuse reflectance spectra of the as-prepared samples are shown in Fig. 3b. Compared with HCNS, the HCNS/AgBr hybrid materials show increased absorption in the UV-visible light region, with HCNS/AgBr60 showing the maximum absorption. This reveals that AgBr loading is favorable for photocatalytic performance. However, the degree of AgBr loading is not proportional to absorption, with the optimal proportion being 60%.

The photoluminescence (PL) spectrum of the pure HCNS and HCNS/AgBr hybrid substances can be seen in Fig. 4a. All samples were measured using an excitation wavelength of $\lambda = 360$ nm and their maximum intensity emission peaks emerged at approximately 480 nm. Addition of silver bromide clearly reduced the PL emission intensity, which could illustrate that the recombination rate of photogenerated charge carriers was restrained for HCNS/AgBr hybrids. It also suggests that the separation efficiency of photogenerated electrons and holes in HCNS/AgBr is better than for pure HCNS.

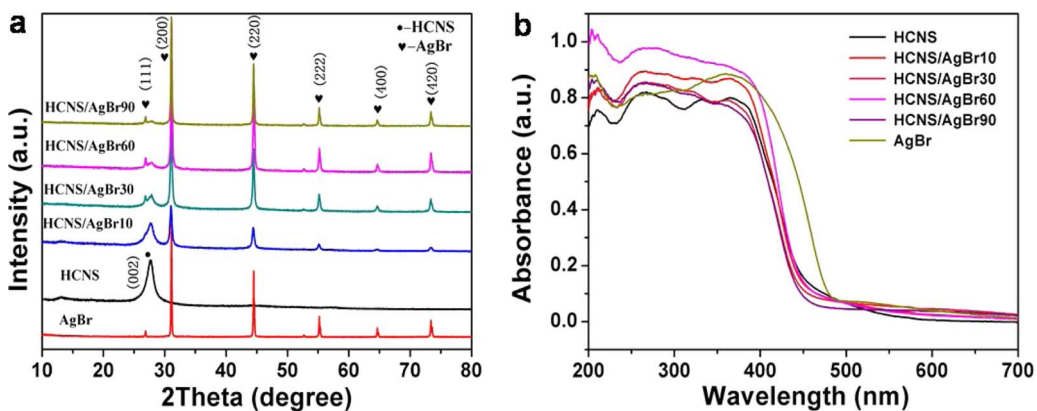
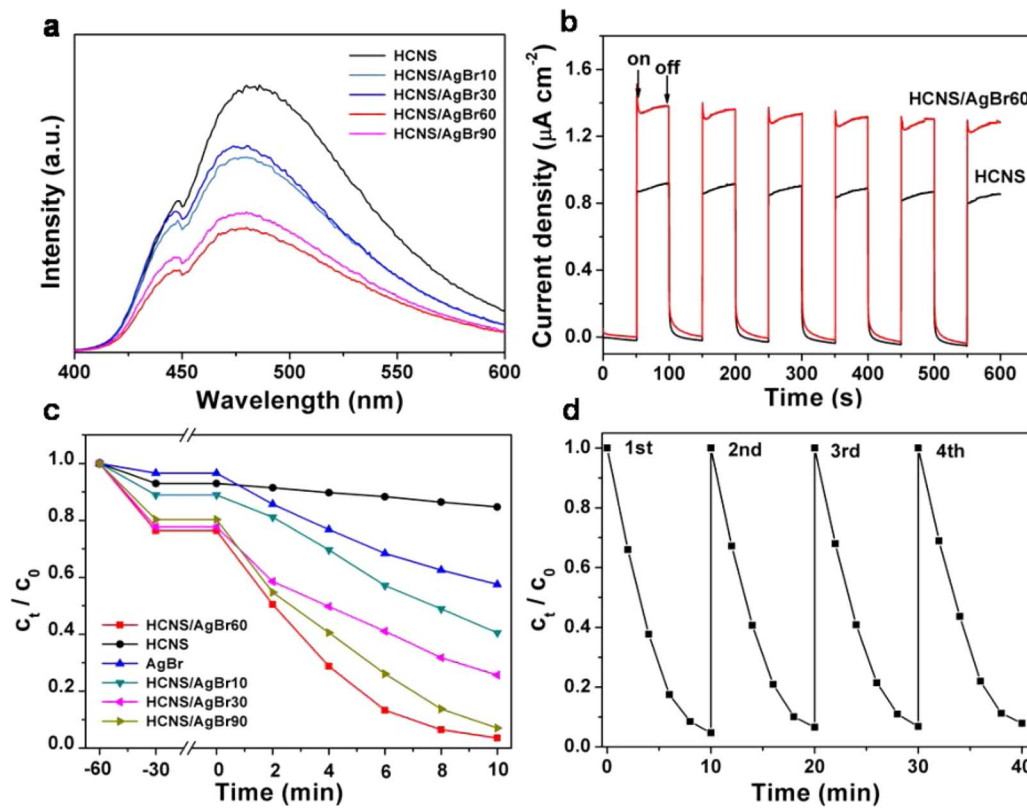


Fig. 3. (a) XRD patterns of HCNS, AgBr and HCNS/AgBr with different mass ratios (b) UV-vis diffuse reflectance spectra of HCNS, AgBr and HCNS/AgBr hybrids.



3.1.4. Electrochemical property

Electrochemical testing was conducted using HCNS or HCNS/AgBr60 as the working electrode. Ag/AgCl and Pt wire were used as the reference and counter electrodes, respectively. The transient photocurrent responses were surveyed under the irradiation of a Xe lamp and six on-off cycles were recorded. The photocurrent time (I-t) diagram shown in Fig. 4b indicates that HCNS/AgBr60 has a much higher photocurrent density than pure HCNS, although both photocurrents show stability and repeatability. Electrochemical testing reveals that photocurrent increased with AgBr loading, which supports the conclusion that HCNS/AgBr hybrids have better separation efficiency of electron and hole, which was reached from analysis of the PL spectrum.

3.2. Photocatalytic studies

3.2.1. Visible-light photocatalytic activity

Catalytic performance is an important parameter in the evaluation of photocatalysts. The photocatalytic activities of HCNS and different mass ratios of HCNS/AgBr materials were evaluated for OG degradation under the same conditions of visible light irradiation. The reaction systems reached absorption-desorption equilibrium after 30 min. Fig. 4c shows that both HCNS and AgBr have low degradation activities of approximately 16% and 40% after 10 min irradiation, respectively. However, addition of AgBr nanoparticles to the HCNS surface resulted in significantly improved photocatalytic effects and rates, particularly for the hybrid containing 60% AgBr. The photocatalytic effect for HCNS/AgBr60 reached approximately 97% within 10 min. Generally speaking, higher ratios of AgBr produced better photocatalytic effects and rates; however, HCNS/AgBr90 did not conform to this trend, showing a decrease compared with HCNS/AgBr60. According to the literature, this observation could be due to the excessive amount of silver bromide destroying the structure of the heterojunction.

3.2.2. Stability and reusability

The potential of a catalyst is also dependent on its stability during

Fig. 4. (a) PL spectra of HCNS and HCNS/AgBr hybrid materials. (b) Transient photocurrent responses of the HCNS and HCNS/AgBr60 samples in 0.1 M Na_2SO_4 aqueous solution under Xe lamp irradiation. (c) Adsorption and photocatalytic activity of HCNS, AgBr and different mass ratios of HCNS/AgBr material in the degradation of OG under visible light irradiation. (d) Cycling run in the photocatalytic reaction process.

the catalytic process. Tests to analyze the stability of the catalysts by repeated recycling were therefore carried out. Recycling was readily achieved by centrifugation to separate out the catalyst, followed by drying at 70°C and multiple washes with water and ethanol. As can be seen in Fig. 4d, the degradation efficiency of the photocatalyst reduced slightly after four cycles; however, stability was maintained. This result illustrates that HCNS/AgBr photocatalysts are reusable and cost-effective. As we all know, silver bromides are unstable under irradiation of light, however, the degradation efficiency just has a slight decline, which is attributed to the generation of metallic Ag° during the photodegradation process (Fig. S3). The XPS spectrum demonstrated that a little metallic Ag° was produced after photodegradation of OG. What's more, the AgBr will be transformed to Ag/AgBr during irradiation, so the mechanism of HCNS/Ag/AgBr was proposed in Fig. S7.

3.3. Kinetics

The photodegradation rates of HCNS, AgBr and different mass ratios of HCNS/AgBr materials were calculated via a pseudo-first-order kinetics model as follows:

$$\ln (C_0/C_t) = kt$$

where C_0 (mg/l) and C_t (mg/l) is the absorption equilibrium concentration of OG and the concentration of OG at the reaction time t (min). The plots of OG concentration versus irradiation time are shown in Fig. 5 and the kinetic data is listed in Table 1. Fig. 5a shows that all of the HCNS/AgBr catalysts revealed higher degradation rate than pure HCNS and AgBr under visible light irradiation. The apparent reaction rate constant k for different mass ratios of HCNS/AgBr, HCNS and AgBr for photodegradation of OG has been calculated from the slope of the kinetic plot and shown in Fig. 5b. It was found that the rate constant k of HCNS/AgBr60 was 0.3442 min^{-1} , which was 40.9 times and 3.28 times as high as that of the pure HCNS and $\text{C}_3\text{N}_4/\text{AgBr60}$ (Fig. S4).

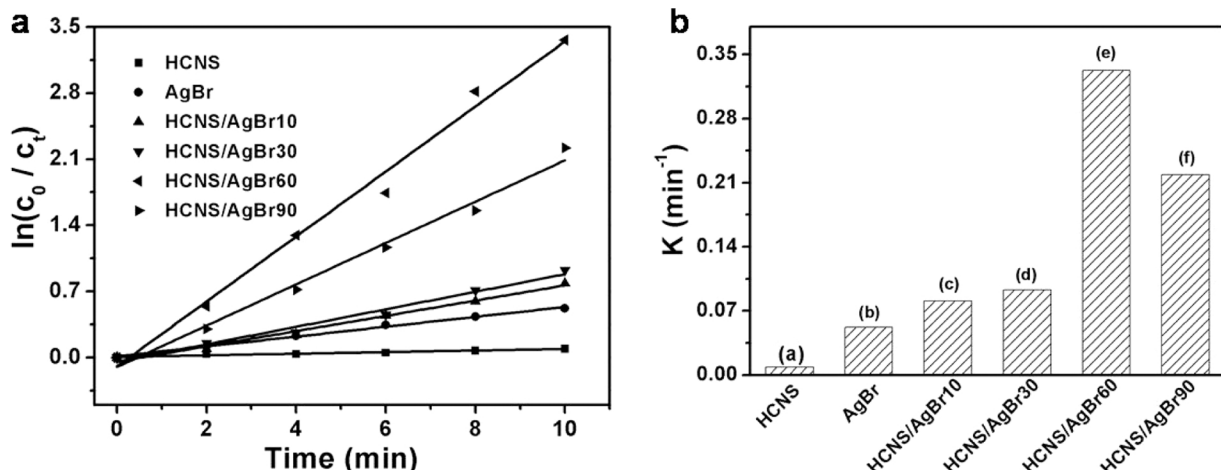


Fig. 5. (a) Kinetic studies of OG degradation with HCNS, AgBr and different mass ratios of HCNS/AgBr materials. (b) Rate constant chart of OG degradation with HCNS, AgBr and different mass ratios of HCNS/AgBr materials.

Table 1
Kinetic constants and correlation coefficients of samples for Orange G photodegradation.

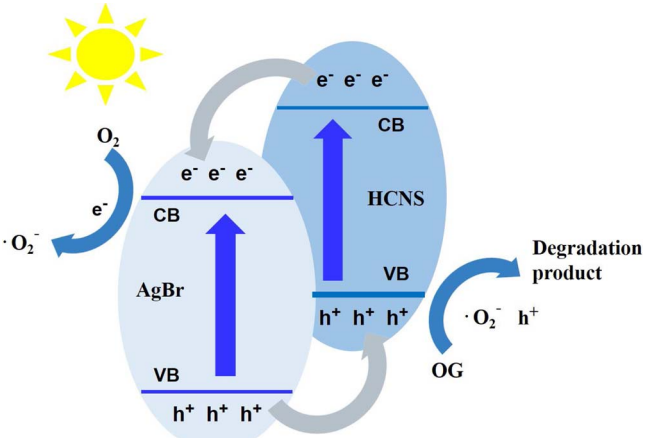
Samples	K (min ⁻¹)	R^2
HCNS	0.0084	0.942
AgBr	0.0522	0.995
HCNS/AgBr10	0.0807	0.988
HCNS/AgBr30	0.0928	0.977
HCNS/AgBr60	0.3442	0.987
HCNS/AgBr90	0.2187	0.984
$C_3N_4/AgBr60$	0.1048	0.999

3.4. Mechanism considerations

3.4.1. Free radical and hole scavenging experiments

Free radical and hole scavenging experiments were carried out in order to understand the active species generated during the process of degradation with HCNS and HCNS/AgBr60. In this study, tert-butyl alcohol (t-BuOH), EDTA and 1, 4-benzoquinone (BQ) are used as the hydroxyl radical ($\cdot OH$) scavenger, hole (h^+) scavenger and superoxide radical ($\cdot O_2^-$) scavenger, respectively.

The influence of various scavengers on the visible light photocatalytic activity of pure HCNS toward the degradation of OG as can be seen in the Fig. 6a. Compared with scavenger-free HCNS photocatalytic system, the degradation rate of OG is hardly inhibited after the addition of t-BuOH (1 mM). As for EDTA (1 mM)-HCNS photocatalytic system, the degradation rate of OG is obviously increased, and in the presence



Scheme 2. Schematic illustration of the OG photodegradation reaction mechanism.

of BQ (1 mM), the degradation of OG is inhibited greatly. The above results indicate that $\cdot OH$ radical is hardly generated, while $\cdot O_2^-$ is the significant active species generated in the HCNS-photocatalytic system. As for h^+ , it can be scavenged in the presence of EDTA, so more e^- can react with O_2 to form $\cdot O_2^-$ instead of the rapid recombination with h^+ (Eq. (2)), which further improves the photocatalytic activity. As for HCNS/AgBr60-photocatalytic system, it shows that $\cdot O_2^-$ is still the main

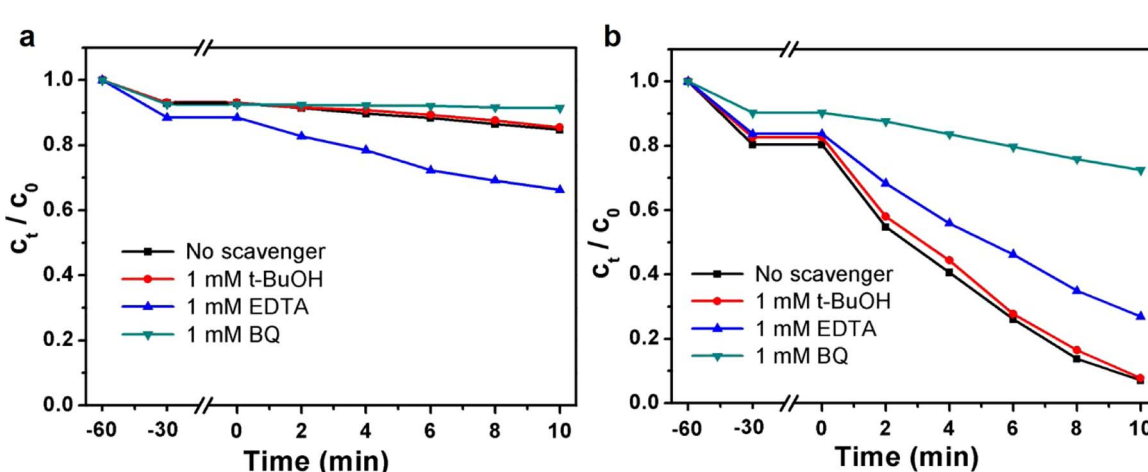


Fig. 6. Influence of various scavengers on the visible light photocatalytic activity of (a) pure HCNS, (b) HCNS/AgBr60 toward the degradation of OG.

Table 2

Degradation times and efficiencies resulting from catalytic photodegradation of OG dye using some reported photocatalysts and HCNS/AgBr.

Photocatalysts	Initial dye concentration (mg L ⁻¹)	Degradation time	Efficiency	Ref.
N-doped TiO ₂ zirconium oxide (Z3)	25	150 min	96.29%	[49]
	20	180 min	100%	[50]
TiO ₂ -carbonxerogel (CTi40)	10	400 min	90%	[51]
TiO ₂ nanotubes/γ-Fe ₂ O ₃	40	90 min	50%	[52]
CuO/Ti ₆ O ₁₃ + H ₂ O ₂	30	15 min	95%	[53]
This work	25	10 min	97%	

active species generated in current system (Fig. 6b). However, ·OH radical is hardly generated in current photocatalytic system [48].

3.4.2. Discussion

Based on previous literature and the above experimental results, the possible photocatalytic mechanism is proposed, as shown in Scheme 2. Before illumination, electrons and holes combine to form electron-hole pairs in the valence band (VB). Under visible light irradiation, electrons are excited to the conduction band (CB) due to absorption of light energy, and the holes are left in the VB band. However, the positively charged holes and the negatively charged electrons attract each other resulting in rapid recombination, and causing the low OG degradation efficiency of HCNS. We therefore propose the formation of a heterojunction structure between AgBr and HCNS, which would lead to the improved catalytic activity observed by increasing the separation efficiency of holes and electrons. In detail, after illumination, the electrons in the CB band of the HCNS spontaneously flow into the CB of AgBr, meanwhile the holes in the VB of AgBr migrate to the VB of the HCNS. The electrons reduce oxygen to ·O₂⁻. Superoxide radicals and holes are both main active species for the degradation of OG dye. In summary, the proposed HCNS/AgBr heterojunction could reduce electron-hole pair recombination and increase efficiency. The whole process can be expressed using the following equations:



To further confirm this mechanism, the electron spin resonance (ESR) spectroscopy were performed to detect the ·O₂⁻ and ·OH, as shown in Fig. S6. The signals of the DMPO-·O₂⁻ species could be observed with dispersion of HCNS/AgBr60 photocatalysts in methanol under visible light irradiation. These results are consistent with the mechanism we have proposed (Table 2).

4. Conclusions

Hollow carbon nitride nanospheres were successfully synthetized using the hard-templating method and AgBr nanoparticles were introduced using the deposition-precipitation method. The HCNS/AgBr hybrids, particularly HCNS/AgBr60, indicate higher photocatalytic efficiency than pure HCNS or AgBr in terms of OG dye degradation. The experimental results show that degradation can be achieved within 10 min, and the degradation efficiency is up to 97%. This is superior to a number of visible-light photocatalysts and is likely due to high electron-hole separation efficiency. The HCNS/AgBr nanocomposites exhibit stability and reusability in the process of photodegradation. In summary, this work demonstrates a high-efficiency photocatalyst for the potential application in the removal of dye from wastewater.

Acknowledgements

We gratefully acknowledge the financial support provided by the National Key R&D Program of China (2017YFC0210901, 2017YFC0210906), National Natural Science Foundation of China (51573122, 21722607, 21776190), Natural Science Foundation of the Jiangsu Higher Education Institutions of China (17KJA430014, 17KJA150009), the Science and Technology Program for Social Development of Jiangsu (BE2015637) and the project supported by the Priority Academic Program Development of Jiangsu Higher Education Institutions (PAPD).

Appendix A. Supplementary data

Supplementary material related to this article can be found, in the online version, at doi:<https://doi.org/10.1016/j.apcatb.2018.02.028>.

References

- [1] J.R. Goldsmith, L.T. Friberg, Effects of air pollution on human health, *Air Pollut.* 2 (1977) 457–610.
- [2] R.P. Schwarzenbach, T. Egli, T.B. Hofstetter, U. von Gunten, B. Wehrli, Global water pollution and human health, *Annu. Rev. Environ. Resour.* 35 (2010) 109–136.
- [3] M. Oliver, Soil and human health: a review, *Eur. J. Soil Sci.* 48 (1997) 573–592.
- [4] R. Kant, Textile dyeing industry an environmental hazard, *Nat. Sci.* 4 (2012) 22.
- [5] J.T. Spadaro, M.H. Gold, V. Renganathan, Degradation of azo dyes by the lignin-degrading fungus *Phanerochaete chrysosporium*, *Appl. Environ. Microbiol.* 58 (1992) 2397–2401.
- [6] I.K. Konstantinou, T.A. Albanis, TiO₂-assisted photocatalytic degradation of azo dyes in aqueous solution: kinetic and mechanistic investigations: a review, *Appl. Catal. B Environ.* 49 (2004) 1–14.
- [7] M.L. Chacón-Patiño, C. Blanco-Tirado, J.P. Hinestrosa, M.Y. Combariza, Biocomposite of nanostructured MnO 2 and fique fibers for efficient dye degradation, *Green Chem.* 15 (2013) 2920–2928.
- [8] M.F.R. Pereira, S.F. Soares, J.J. Órfão, J.L. Figueiredo, Adsorption of dyes on activated carbons: influence of surface chemical groups, *Carbon* 41 (2003) 811–821.
- [9] K. Jain, V. Shah, D. Chapla, D. Madamwar, Decolorization and degradation of azo dye-Reactive Violet 5R by an acclimated indigenous bacterial mixed cultures-SB4 isolated from anthropogenic dye contaminated soil, *J. Hazard. Mater.* 213 (2012) 378–386.
- [10] H. Awad, N.A. Galwa, Electrochemical degradation of Acid Blue and Basic Brown dyes on Pb/PbO₂ electrode in the presence of different conductive electrolyte and effect of various operating factors, *Chemosphere* 61 (2005) 1327–1335.
- [11] H. Lachheb, E. Puzenat, A. Houas, M. Ksibi, E. Elaloui, C. Guillard, J.-M. Herrmann, Photocatalytic degradation of various types of dyes (Alizarin S, Crocein Orange G, Methyl Red, Congo Red, Methylene Blue) in water by UV-irradiated titania, *Appl. Catal. B Environ.* 39 (2002) 75–90.
- [12] L. Liu, Z. Ji, W. Zou, X. Gu, Y. Deng, F. Gao, C. Tang, L. Dong, In situ loading transition metal oxide clusters on TiO₂ nanosheets as co-catalysts for exceptional high photoactivity, *ACS Catal.* 3 (2013) 2052–2061.
- [13] L. Liu, X. Gu, Z. Ji, W. Zou, C. Tang, F. Gao, L. Dong, Anion-assisted synthesis of TiO₂ nanocrystals with tunable crystal forms and crystal facets and their photocatalytic redox activities in organic reactions, *J. Phys. Chem. C* 117 (2013) 18578–18587.
- [14] N. Daneshvar, D. Salari, A. Khataee, Photocatalytic degradation of azo dye acid red 14 in water on ZnO as an alternative catalyst to TiO₂, *J. Photochem. Photobiol. A* 162 (2004) 317–322.
- [15] F. Xu, Y. Shen, L. Sun, H. Zeng, Y. Lu, Enhanced photocatalytic activity of hierarchical ZnO nanoplate-nanowire architecture as environmentally safe and facilely recyclable photocatalyst, *Nanoscale* 3 (2011) 5020–5025.
- [16] C. Pan, Y. Zhu, New type of BiPO₄ oxy-acid salt photocatalyst with high photocatalytic activity on degradation of dye, *Environ. Sci. Technol.* 44 (2010) 5570–5574.
- [17] A.G. Prado, L.B. Bolzon, C.P. Pedroso, A.O. Moura, L.L. Costa, Nb₂O₅ as efficient and recyclable photocatalyst for indigo carmine degradation, *Appl. Catal. B Environ.* 82 (2008) 219–224.
- [18] S. Anandan, G.-J. Lee, P.-K. Chen, C. Fan, J.J. Wu, Removal of orange II dye in water by visible light assisted photocatalytic ozonation using Bi₂O₃ and Au/Bi₂O₃ nanorods, *Ind. Eng. Chem. Res.* 49 (2010) 9729–9737.
- [19] F. Dong, W.-K. Ho, S. Lee, Z. Wu, M. Fu, S. Zou, Y. Huang, Template-free fabrication and growth mechanism of uniform (BiO)₂CO₃ hierarchical hollow microspheres with outstanding photocatalytic activities under both UV and visible light irradiation, *J. Mater. Chem.* 21 (2011) 12428–12436.
- [20] Q. Wei, Z. Zhang, Z. Li, Q. Zhou, Y. Zhu, Enhanced photocatalytic activity of porous α-Fe₂O₃ films prepared by rapid thermal oxidation, *J. Phys. D Appl. Phys.* 41 (2008) 202002.
- [21] X. Zhou, Q. Xu, W. Lei, T. Zhang, X. Qi, G. Liu, K. Deng, J. Yu, Origin of tunable photocatalytic selectivity of well-defined α-Fe₂O₃ nanocrystals, *Small* 10 (2014) 674–679.
- [22] J. Liu, T. Zhang, Z. Wang, G. Dawson, W. Chen, Simple pyrolysis of urea into

graphitic carbon nitride with recyclable adsorption and photocatalytic activity, *J. Mater. Chem.* 21 (2011) 14398–14401.

[23] Y. Liu, X. Chen, J. Li, C. Burda, Photocatalytic degradation of azo dyes by nitrogen-doped TiO_2 nanocatalysts, *Chemosphere* 61 (2005) 11–18.

[24] P. Sathishkumar, S. Anandan, P. Maruthamuthu, T. Swaminathan, M. Zhou, M. Ashokkumar, Synthesis of Fe^{3+} doped TiO_2 photocatalysts for the visible assisted degradation of an azo dye, *Colloids Surf. A Physicochem. Eng. Asp.* 375 (2011) 231–236.

[25] Z. Xiong, L.L. Zhang, J. Ma, X. Zhao, Photocatalytic degradation of dyes over graphene–gold nanocomposites under visible light irradiation, *Chem. Commun.* 46 (2010) 6099–6101.

[26] R. Ullah, J. Dutta, Photocatalytic degradation of organic dyes with manganese-doped ZnO nanoparticles, *J. Hazard. Mater.* 156 (2008) 194–200.

[27] X. Zhang, L. Zhang, T. Xie, D. Wang, Low-temperature synthesis and high visible-light-induced photocatalytic activity of BiOI/TiO_2 heterostructures, *J. Phys. Chem. C* 113 (2009) 7371–7378.

[28] W. Zou, L. Zhang, L. Liu, X. Wang, J. Sun, S. Wu, Y. Deng, C. Tang, F. Gao, L. Dong, Engineering the Cu_2O -reduced graphene oxide interface to enhance photocatalytic degradation of organic pollutants under visible light, *Appl. Catal. B Environ.* 181 (2016) 495–503.

[29] W. Zou, Y. Shao, Y. Pu, Y. Luo, J. Sun, K. Ma, C. Tang, F. Gao, L. Dong, Enhanced visible light photocatalytic hydrogen evolution via cubic CeO_2 hybridized $\text{g-C}_3\text{N}_4$ composite, *Appl. Catal. B Environ.* 218 (2017) 51–59.

[30] H. Xu, J. Yan, Y. Xu, Y. Song, H. Li, J. Xia, C. Huang, H. Wan, Novel visible-light-driven $\text{AgX}/\text{graphite-like C}_3\text{N}_4$ ($\text{X} = \text{Br, I}$) hybrid materials with synergistic photocatalytic activity, *Appl. Catal. B Environ.* 129 (2013) 182–193.

[31] S. Cao, J. Yu, $\text{g-C}_3\text{N}_4$ -based photocatalysts for hydrogen generation, *J. Phys. Chem. Lett.* 5 (2014) 2101–2107.

[32] X. Wang, S. Blechert, M. Antonietti, Polymeric graphitic carbon nitride for heterogeneous photocatalysis, *ACS Catal.* 2 (2012) 1596–1606.

[33] J. Low, S. Cao, J. Yu, S. Wageh, Two-dimensional layered composite photocatalysts, *Chem. Commun.* 50 (2014) 10768–10777.

[34] G. Dong, W. Ho, Y. Li, L. Zhang, Facile synthesis of porous graphene-like carbon nitride ($\text{C}_6\text{N}_4\text{H}_3$) with excellent photocatalytic activity for NO removal, *Appl. Catal. B Environ.* 174 (2015) 477–485.

[35] J. Fang, H. Fan, M. Li, C. Long, Nitrogen self-doped graphitic carbon nitride as efficient visible light photocatalyst for hydrogen evolution, *J. Mater. Chem. A* 3 (2015) 13819–13826.

[36] J. Liu, W. Li, L. Duan, X. Li, L. Ji, Z. Geng, K. Huang, L. Lu, L. Zhou, Z. Liu, A graphene-like oxygenated carbon nitride material for improved cycle-life lithium/sulfur batteries, *Nano Lett.* 15 (2015) 5137–5142.

[37] X. Song, Y. Hu, M. Zheng, C. Wei, Solvent-free *in situ* synthesis of $\text{g-C}_3\text{N}_4/\{001\}$ TiO_2 composite with enhanced UV-and visible-light photocatalytic activity for NO oxidation, *Appl. Catal. B Environ.* 182 (2016) 587–597.

[38] J. Yu, K. Wang, W. Xiao, B. Cheng, Photocatalytic reduction of CO_2 into hydrocarbon solar fuels over $\text{g-C}_3\text{N}_4$ –Pt nanocomposite photocatalysts, *Phys. Chem. Chem. Phys.* 16 (2014) 11492–11501.

[39] K. Wang, Q. Li, B. Liu, B. Cheng, W. Ho, J. Yu, Sulfur-doped $\text{g-C}_3\text{N}_4$ with enhanced photocatalytic CO_2 -reduction performance, *Appl. Catal. B Environ.* 176 (2015) 44–52.

[40] K. Maeda, X. Wang, Y. Nishihara, D. Lu, M. Antonietti, K. Domen, Photocatalytic activities of graphitic carbon nitride powder for water reduction and oxidation under visible light, *J. Phys. Chem. C* 113 (2009) 4940–4947.

[41] J. Liu, H. Wang, Z.P. Chen, H. Moehwald, S. Fiechter, R. van de Krol, L. Wen, L. Jiang, M. Antonietti, Microcontact-printing-assisted access of graphitic carbon nitride films with favorable textures toward photoelectrochemical application, *Adv. Mater.* 27 (2015) 712–718.

[42] G. Zhang, M. Zhang, X. Ye, X. Qiu, S. Lin, X. Wang, Iodine modified carbon nitride semiconductors as visible light photocatalysts for hydrogen evolution, *Adv. Mater.* 26 (2014) 805–809.

[43] Y. Cui, G. Zhang, Z. Lin, X. Wang, Condensed and low-defected graphitic carbon nitride with enhanced photocatalytic hydrogen evolution under visible light irradiation, *Appl. Catal. B Environ.* 181 (2016) 413–419.

[44] D.M. Teter, R.J. Hemley, Low-compressibility carbon nitrides, *Science* 271 (1996) 53.

[45] Y. Zhao, J. Zhang, L. Qu, Graphitic carbon nitride/graphene hybrids as new active materials for energy conversion and storage, *ChemNanoMat* 1 (2015) 298–318.

[46] J. Sun, J. Zhang, M. Zhang, M. Antonietti, X. Fu, X. Wang, Bioinspired hollow semiconductor nanospheres as photosynthetic nanoparticles, *Nat. Commun.* (2012) 1139.

[47] H. Li, S. Gan, H. Wang, D. Han, L. Niu, Intercorrelated superhybrid of AgBr supported on graphitic C_3N_4 -decorated nitrogen-doped graphene: high engineering photocatalytic activities for water purification and CO_2 reduction, *Adv. Mater.* 27 (2015) 6906–6913.

[48] Y. Yang, W. Guo, Y. Guo, Y. Zhao, X. Yuan, Y. Guo, Fabrication of Z-scheme plasmonic photocatalyst $\text{Ag}@\text{AgBr}/\text{g-C}_3\text{N}_4$ with enhanced visible-light photocatalytic activity, *J. Hazard. Mater.* 271 (2014) 150–159.

[49] J. Sun, L. Qiao, S. Sun, G. Wang, Photocatalytic degradation of Orange G on nitrogen-doped TiO_2 catalysts under visible light and sunlight irradiation, *J. Hazard. Mater.* 155 (2008) 312–319.

[50] I.M. Ibrahim, M.E. Moustafa, M.R. Abdelhamid, Effect of organic acids precursors on the morphology and size of ZrO_2 nanoparticles for photocatalytic degradation of Orange G dye from aqueous solutions, *J. Mol. Liq.* 223 (2016) 741–748.

[51] E. Bailón-García, A. Elmouwahidi, M.A. Álvarez, F. Carrasco-Marín, A.F. Pérez-Cadenas, F.J. Maldonado-Hódar, New carbon xerogel- TiO_2 composites with high performance as visible-light photocatalysts for dye mineralization, *Appl. Catal. B Environ.* 201 (2017) 29–40.

[52] Y.L. Pang, S. Lim, H.C. Ong, W.T. Chong, Synthesis, characteristics and sonocatalytic activities of calcined gamma- Fe_2O_3 and TiO_2 nanotubes/gamma- Fe_2O_3 magnetic catalysts in the degradation of Orange G, *Ultrason. Sonochem.* 29 (2016) 317–327.

[53] S. Sehati, M.H. Entezari, Sono-incorporation of CuO nanoparticles on the surface and into the mesoporous hexatitanate layers: enhanced fenton-like activity in degradation of orange-G at its neutral pH, *Appl. Surf. Sci.* 399 (2017) 732–741.